Multiple-Post Inductive Obstacles in Rectangular Waveguide

PING GUAN LI, ARLON T. ADAMS, SENIOR MEMBER, IEEE, YEHUDA LEVIATAN, MEMBER, IEEE, AND JOSE PERINI, SENIOR MEMBER, IEEE

Abstract—A complete analysis of multiple-post inductive obstacles in rectangular waveguide is presented. A moment method solution with exponential ($e^{jn\theta}$) expansion and weighting functions is used in a Galerkin solution. Post currents are expressed as a Fourier series. As many Fourier series terms ($e^{jn\theta}$) as desired may be included. All higher order (cutoff) mode interactions between posts are taken into account. The solution is rapid and accurate, and errors may be controlled (specified). Data are given for the triple-post obstacle and for a two-element filter.

I. Introduction

THE CYLINDRICAL POST in a rectangular waveguide was first treated by the well-known and widely referenced variational method of Schwinger [1], and the results are given in Marcuvitz's *Waveguide Handbook* [2]. Fig. 1 shows the geometry and a cylindrical coordinate system centered at the post axis. A dominant mode is incident upon the post which is assumed to be a perfect conductor. The currents induced on the post are longitudinally directed (parallel to the post axis) and vary circumferentially. There is no longitudinal variation of the currents. The post currents thus may be represented in terms of a Fourier series $\Sigma_{-\infty}^{\infty} A_n e^{jn\theta}$. Schwinger had taken into account the zeroth and first-order terms of the series in his variational solution. The results were limited to posts which were moderate in size and distant from each other and from the waveguide walls, but very accurate within those limitations. The results were useful in the design of microwave post filters.

Craven and Lewin [3], [4] pointed out the advantages of a triple-post configuration, such as that of Fig. 3, in suppressing higher order modes. Mariani [5] analyzed the triple-post configuration, but found it necessary to add experimentally determined correction factors.

Recent work with inductive posts includes that of Abele [6] and Moschinskiy and Berezovskiy [7]. Abele treats the symmetrical-post arrangement. Moschinskiy and Berezovskiy use a doubly infinite set of linear equations. Neither treats higher order mode interactions. Posts with gaps have been treated by a number of authors, including Joshi and Cornick [8], Eisenhart and Kahn [9], Hicks and Khan [10], and Williamson and Otto [11]. Ferrimagnetic posts have been treated by Okamoto *et al.* [12], and inductive strips have been treated by several authors [4], [13], and [14].

Manuscript received June 1, 1983; revised November 15, 1983.

The authors are with the Department of Electrical and Computer Engineering, Syracuse University, Syracuse, NY 13210.

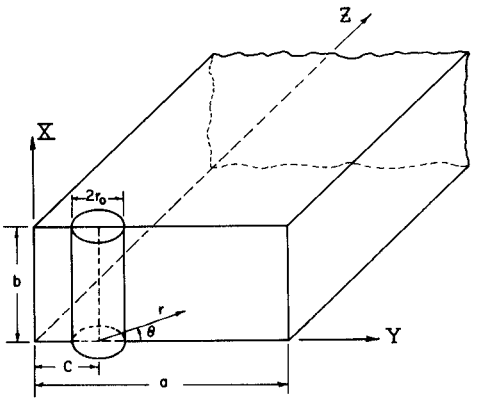

Fig. 1. A single-post obstacle in a rectangular waveguide.

As time went by, filters of higher Q were desired. These could be obtained by using either larger posts or a multiple-post configuration, such as that of Fig. 3. For either of these choices, it is necessary to take into account the higher order terms of the Fourier series. This paper uses a method of moments [15] solution to the single- and triple-post problems and to arrays of such post configurations. Exponential expansion ($e^{jn\theta}$) and weighting functions [15] are used in a Galerkin solution, which is also variational. The complete formulation is developed for all terms of the Fourier series. The series is truncated at $n = \pm N$ and a matrix equation is obtained for the unknown coefficients of the Fourier series. The convergence of the solution is studied as a function of the number of terms used. In some cases, terms were required for N as large as five.

The solution utilizes an infinite series of images (Fig. 2) of the post currents to obtain the electric fields in the waveguide. Thus, fields are represented in terms of free-space post currents. The scattered fields are expressed in terms of a single polar coordinate system through the use of the addition theorem of the Hankel function. Incident fields are also expressed in terms of the same polar coordinate system. The application of the boundary conditions at the post then yields the complete equations which, when truncated at $n = \pm N$, represent a system of $2N+1$ unknowns, which may be expressed as the matrix equation

$$[c] = [H][a].$$

Because of the use of image fields, the elements of the matrix are each represented as infinite series which converge very slowly. A method is found which enables us to

0018-9480/84/0400-0365$01.00 ©1984 IEEE

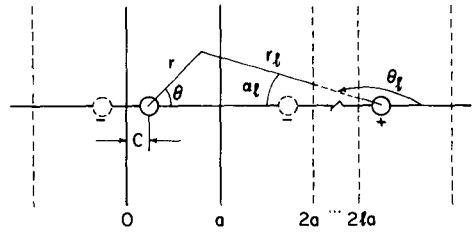

Fig. 2. Images of the single post.

sum the real part of the elements of $[H]$ in closed form. The imaginary part is changed to a form involving both proper and improper integrals. Both are evaluated numerically. A method is developed for estimating and specifying (controlling) the errors involved in the numerical evaluations. The computation is very rapid and the errors due to numerical evaluation may be specified. There are three sources of error: a) the evaluation of the proper integrals, b) the evaluation of the improper integrals, and c) the truncation at $n = \pm N$. The first two sources are controlled by specifying error levels, and the last is evaluated by varying N and observing convergence.

Once the post currents (coefficients of the Fourier series) are obtained, the total scattered fields, transmission and reflection coefficients, and equivalent circuits may be readily obtained. The data for single posts of moderate size plot right on top of Marcuvitz's data. The data for larger posts, and for those near the waveguide wall, agree within a fraction of one percent with data obtained from a multifilament approximation described in a previous paper [16]. The triple-post data also agree precisely with that obtained by the filamentary model.

Each of the two models used has its advantages. The Fourier series current model is variational, requires fewer unknowns, and is particularly suitable for cylindrical-post geometries of all types. The multifilament model is simpler and may be more generally useful in the characterization of obstacles of arbitrary shape.

For triple-post configurations, such as that of Fig. 3, the formulation is quite similar to that of the single post. For arrays of posts with separation in the direction of propagation, the formulation is quite different. For the most accurate results, higher order waveguide mode interactions must be taken into account. In this case, the elements of $[H]$ are of a more complex form. Methods are used again, to reduce these forms to those suitable for computations; both the real and imaginary parts are expressed as integrals, which are evaluated numerically. Again, the errors involved are controlled by specification. Fig. 4 shows the in-line case (post-centers have identical y coordinates). Post arrays with non-in-line elements also can be treated by similar methods.

As a result of the formulation developed, one may treat arrays of posts in a rectangular waveguide, taking into account as many terms of the Fourier series for the currents as desired, and taking into account all higher order mode interactions between posts. Asymmetrical post configurations may be treated; for example, the off-center post data of [16] was calculated by both the Fourier series surface current and the filamentary current models. Results are presented for the equivalent circuits of triple-post configurations and for the filter response of a two-element post filter.

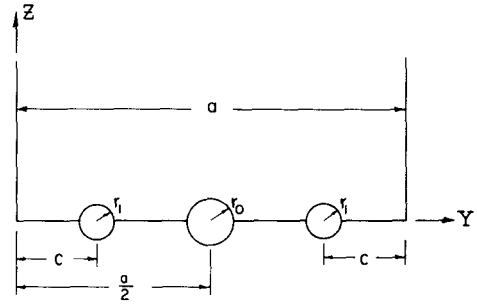

Fig. 3. A triple-post obstacle in a rectangular waveguide.

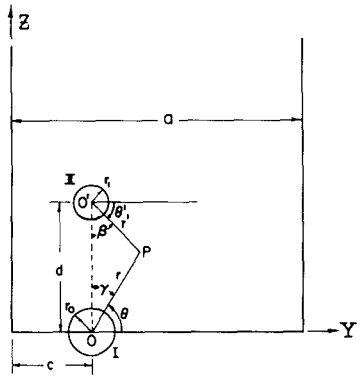

Fig. 4. A single-post array in a rectangular waveguide.

II. The Basic Formulation

In this section, the basic formulation for the single-post is presented, and the formulations for the triple-post configuration and for the post array are summarized. In each case, a matrix equation is obtained for the post currents.

A. Single-Post Obstacle

Fig. 1 shows a rectangular inductive post in a rectangular waveguide. Dominant mode fields are incident. A dominant mode traveling in the z direction is incident upon the post. A cylindrical coordinate system is centered on the post axis at $z = 0$, $y = c$. The incident electric field E_x^i may be expressed as follows:

$$E_x^i = E_0 e^{-\imath k' z} \sin\left(\frac{\pi y}{a}\right) \tag{1}$$

where

$$k' = \sqrt{k^2 - \pi^2/a^2} = \frac{2\pi}{\lambda g} \quad \text{and} \quad k = \frac{2\pi}{\lambda}.$$

The incident wave can be expressed in Fourier series form. Substitution of $y = c + r\cos\theta$ and $z = r\sin\theta$ into (1)

yields

$$E_x^i = E_0 e^{-jk'r\sin\theta}\sin\left[\frac{\pi(c+r\cos\theta)}{a}\right] = \frac{E_0}{2j}\left\{e^{j[(\pi c/a)-kr\sin(\theta-\alpha)]} - e^{-j[(\pi c/a)+kr\sin(\theta+\alpha)]}\right\} \tag{2}$$

where

$$\alpha = \tan^{-1}\left(\frac{\pi}{k'a}\right).$$

The generation function for the Bessel function is [17]

$$e^{(x/2)(t-t^{-1})} = \sum_{n=-\infty}^{\infty} J_n(x)t^n.$$

Let $t = e^{j\theta}$, $x = kr$, and the generation function becomes

$$e^{jkr\sin\theta} = \sum_{n=-\infty}^{\infty} J_n(kr)e^{jn\theta}. \tag{3}$$

Replacement of θ with $\theta \pm \alpha$ in (3) and substitution of (3) into (2) yields the desired Fourier series form

$$E_x^i = \sum_{n=-\infty}^{\infty} E_0\sin\left(\frac{\pi c}{a}+n\alpha\right)J_n(kr)e^{-jn\theta} = \sum_{n=-\infty}^{\infty}(-1)^n E_0\sin\left(\frac{\pi c}{a}-n\alpha\right)J_n(kr)e^{jn\theta}. \tag{4}$$

The post surface current density may be represented as

$$J_x(\theta) = \sum_{n=-\infty}^{\infty} a_n' e^{jn\theta}. \tag{5}$$

Thus, full-domain expansion functions $e^{jn\theta}$ have been used for the post surface current. Identical weighting functions are used later, resulting in a Galerkin or variational solution [15].

The post currents now may be imaged across waveguide walls. Imaging across horizontal walls ($x = 0, b$) yields a cylinder of infinite length. The fields in free space due to the currents of (5) on a cylinder of infinite length in free space are

$$E_x = \sum_{n=-\infty}^{\infty} a_n H_n^{(2)}(kr)e^{jn\theta} \tag{6}$$

where the coefficients $\{a_n\}$ and $\{a_n'\}$ are related [18] by

$$a_n' = -\frac{2\omega\varepsilon}{k^2\pi r_0 J_n(kr_0)}a_n. \tag{7}$$

Imaging across vertical waveguide walls yields an infinite number of such cylinders in free space (Fig. 2). The total scattered electric field (the field due to post and image currents) may be expressed as

$$E_x^s = E_x^{\text{post}} + E_x^{\text{images}(+)} + E_x^{\text{images}(-)} \tag{8}$$

where images ($\pm$) represent images with currents identical, opposite, respectively, to post currents. Thus

$$E_x^{\text{images}(+)} = \sum_{\substack{l=-\infty \\ l\neq 0}}^{\infty}\sum_{m=-\infty}^{\infty} a_m H_m^{(2)}(kr_l)e^{jm\theta_l} = \sum_{\substack{l=-\infty \\ l\neq 0}}^{\infty}\sum_{m=-\infty}^{\infty} a_m H_{-m}^{(2)}(kr_l)e^{-jm\alpha_l}. \tag{9}$$

The addition theorem of the Hankel function [19] allows us to represent the above results in terms of the cylindrical coordinate system of Fig. 1, for $r < 2a$

$$E_x^{\text{images}(+)} = \sum_{\substack{l=-\infty \\ l\neq 0}}^{\infty}\sum_{m=-\infty}^{\infty} a_m \sum_{n=-\infty}^{\infty} H_{n-m}^{(2)}(k2la)J_n(kr)e^{jn\theta} \tag{10}$$

and for $r < 2c$

$$E_x^{\text{images}(-)} = -\sum_{l=-\infty}^{\infty}\sum_{m=-\infty}^{\infty} a_m \sum_{n=-\infty}^{\infty} H_{n+m}^{(2)}[k(2la-2c)]J_n(kr)e^{jn\theta}. \tag{11}$$

At the surface of the post, the total electric field must be zero, i.e.,

$$E_x^s(r=r_0) + E_x^i(r=r_0) = 0. \tag{12}$$

Substitution of (4), (6), (10), and (11) into (12) yields an equation with triple sums. Multiplying that result by a weighting function $e^{-jn'\theta}$ and integrating from 0 to 2π in θ yields by orthogonality the following equation:

$$a_n H_n^{(2)}(kr_0) + \sum_{m=-\infty}^{\infty} a_m\left\{\sum_{\substack{l=-\infty \\ l\neq 0}}^{\infty} H_{n-m}^{(2)}(k2la) - \sum_{l=-\infty}^{\infty} H_{n+m}^{(2)}[k(2la-2c)]\right\} \cdot J_n(kr_0) + (-1)^n E_0\sin\left(\frac{\pi c}{a}-n\alpha\right)J_n(kr_0) = 0. \tag{13}$$

The current is now approximated by a finite number of expansion functions, and (13) can be written in the following matrix form:

$$[c] = [H][a] \tag{14}$$

where matrix $[H] = \{h_{ij} | i, j = -N, \cdots, -1, 0, 1, \cdots, N\}$ is described by

$$h_{ij} = \delta_{ij}H_i^{(2)}(kr_0) + \left\{\sum_{\substack{l=-\infty \\ l\neq 0}}^{\infty} H_{i-j}^{(2)}(k2la) - \sum_{l=-\infty}^{\infty} H_{i+j}^{(2)}[k(2la-2c)]\right\}J_i(kr_0) \tag{15}$$

and where δ_{ij} is the Kronecker Delta

$$\delta_{ij} = \begin{cases} 1 & i = j \\ 0 & i \neq j \end{cases}$$

and

$$\text{vector } [c] = \{c_i\} \qquad (i = -N, \cdots, -1, 0, 1, \cdots, N)$$

$$c_i = (-1)^{i+1} E_0 \sin\left(\frac{\pi c}{a} - i\alpha\right) J_i(kr_0) \tag{16}$$

and

$$\text{vector } [a] = \{a_n\} \qquad (n = -N, \cdots, -1, 0, 1, \cdots, N).$$

Thus, expansion and weighting functions $e^{jn\theta}$ have been used where $-N \leqslant n \leqslant N$. N may be varied to study convergence of the solution.

Note that a slightly unusual definition of matrix $[H]$ has been employed in which the subscripts can be zero or negative integers

$$[H] = \begin{bmatrix} h_{-N,-N} & \cdots & h_{-N,N} \\ & \ddots & \\ \vdots & H_{0,0} & \vdots \\ & \ddots & \\ h_{N,-N} & \cdots & h_{N,N} \end{bmatrix}.$$

B. Triple-Post Configuration

The triple-post configuration shown in Fig. 3 is often used in microwave filter design. This configuration can be treated by a method similar to that of the single post. The results will be summarized here. They are given in detail in [20].

Assume that a dominant mode is incident upon the symmetrical triple-post configuration of Fig. 3. The induced current density on the centered post is

$$J_{xc}(\theta) = \sum_{n=-\infty}^{\infty} a'_n e^{jn\theta} \tag{17}$$

and that on the left-hand post is

$$J_{xl}(\theta) = \sum_{n=-\infty}^{\infty} b'_n e^{jn\theta}. \tag{18}$$

Then, by symmetry, the current on the right-hand post is

$$J_{xr}(\theta) = \sum_{n=-\infty}^{\infty} b'_n e^{jn(\pi-\theta)} = \sum_{n=-\infty}^{\infty} (-1)^n b'_n e^{-jn\Theta}. \tag{19}$$

Imaging as before across the horizontal wall yields three cylinders of infinite length. The corresponding free-space fields due to these cylinders with currents (17), (18), and (19) are, respectively

$$E_{xc} = \sum_{n=-\infty}^{\infty} a_n H_n^{(2)}(kr) e^{jn\theta} \tag{20}$$

$$E_{xl} = \sum_{n=-\infty}^{\infty} b_n H_n^{(2)}(kr) e^{jn\theta} \tag{21}$$

$$E_{xr} = \sum_{n=-\infty}^{\infty} b_n H_n^{(2)}(kr) e^{jn(\pi-\theta)} = \sum_{n=-\infty}^{\infty} (-1)^n b_n H_n^{(2)}(kr) e^{-jn\Theta}. \tag{22}$$

Primed and unprimed coefficients are related by (7), as before.

Boundary conditions are applied at the center post and at one of the other posts. The result is a matrix equation.

$$\left[\begin{array}{c|c} [H^{(1)}] & [H^{(2)}] \\ \hline [H^{(3)}] & [H^{(4)}] \end{array}\right] \left[\begin{array}{c} [a] \\ \hline [b] \end{array}\right] = \left[\begin{array}{c} [c^a] \\ \hline [c^b] \end{array}\right] \tag{23}$$

or

$$[c] = [H] \left[\begin{array}{c} [a] \\ [b] \end{array}\right]$$

where

$$h_{ij}^{(1)} = \delta_{ij} H_i^{(2)}(kr_0) + \left[\sum_{\substack{m=-\infty \\ m \neq 0}}^{\infty} H_{i-j}^{(2)}(m2ka) - \sum_{m=-\infty}^{\infty} H_{i+j}^{(2)}(m2ka + ka) \right] J_i(kr_0) \tag{24}$$

$$h_{ij}^{(2)} = \sum_{m=-\infty}^{\infty} \left[H_{i-j}^{(2)}\left(m2ka - \left(\tfrac{1}{2}ka - kc\right)\right) - H_{i+j}^{(2)}\left(m2ka - \left(\tfrac{1}{2}ka + kc\right)\right) + H_{i+j}^{(2)}\left(m2ka + \left(\tfrac{1}{2}ka - kc\right)\right) - H_{i-j}^{(2)}\left(m2ka + \left(\tfrac{1}{2}ka + kc\right)\right) \right] J_i(kr_0) \tag{25}$$

$$c_i^a = (-1)^{i+1} E_0 \cos(i\alpha) J_i(kr_0) \tag{26}$$

$$h_{ij}^{(3)} = \sum_{m=-\infty}^{\infty} \left[H_{i-j}^{(2)}\left(m2ka + \left(\tfrac{1}{2}ka - kc\right)\right) - H_{i+j}^{(2)}\left(m2ka - \left(\tfrac{1}{2}ka + kc\right)\right) \right] J_n(kr_1) \tag{27}$$

$$h_{ij}^{(4)} = \delta_{ij} H_i^{(2)}(kr_1) + \left[\sum_{\substack{m=-\infty \\ m \neq 0}}^{\infty} H_{i-j}^{(2)}(m2ka) - \sum_{m=-\infty}^{\infty} H_{i+j}^{(2)}(m2ka - 2kc) + \sum_{m=-\infty}^{\infty} H_{i+j}^{(2)}(m2ka + (ka - 2kc)) - \sum_{m=-\infty}^{\infty} H_{i-j}^{(2)}(m2ka + ka) \right] J_i(kr_1) \tag{28}$$

$$c_i^b = (-1)^{i+1} E_0 \sin\left(\frac{\pi c}{a} - i\alpha\right) J_i(kr_1). \tag{29}$$

Matrices $[a],[b]$ represent coefficients of (20), (21) where $-N \leqslant n \leqslant N$. Thus, all square matrices $[H^{(i)}]$ of (23) are $2N+1$ by $2N+1$ and all column matrices $[a],[b],[c^a],[c^b]$ are $2N+1$ element columns.

C. Single-Post Array

Fig. 4 shows two posts whose axes are identical y coordinates and different z coordinates, i.e., they are separated in the direction of propagation. A dominant mode is incident upon the posts. Post currents are represented as follows:

$$J_x^{(0)}(\theta) = \sum_{n=-\infty}^{\infty} a_n' e^{jn\theta} \tag{30}$$

$$J_x^{(1)}(\theta') = \sum_{n=-\infty}^{\infty} b_n' e^{jn\theta'} \tag{31}$$

and electric fields due to the corresponding infinite cylinders in free space are

$$E_x^{(0)} = \sum_{n=-\infty}^{\infty} a_n H_n^{(2)}(kr) e^{jn\theta} \tag{32}$$

$$E_x^{(1)} = \sum_{n=-\infty}^{\infty} b_n H_n^{(2)}(kr') e^{jn\theta'}. \tag{33}$$

Primed and unprimed coefficients are related by (7).

The incident fields may be expressed in terms of either polar coordinate system

$$E_x^i = \sum_{n=-\infty}^{\infty} (-1)^n E_0 \sin\left(\frac{\pi c}{a} - n\alpha\right) J_n(kr) e^{jn\theta} \tag{34}$$

$$E_x^i = \sum_{n=-\infty}^{\infty} (-1)^n E_0 e^{-jk'd} \sin\left(\frac{\pi c}{a} - n\alpha\right) J_n(kr') e^{jn\theta'} \tag{35}$$

where

$$\alpha = \tan^{-1}\left(\frac{\pi}{k'a}\right) = \sin^{-1}\left(\frac{\pi}{ka}\right) = \cos^{-1}\left(\frac{k'}{k}\right).$$

The addition theorem for Hankel functions is applied as before. A transformation of coordinates from one polar coordinate system to the other is also required. Boundary conditions are applied at each post and orthogonality is invoked, resulting in a matrix for the coefficients which is identical in form to (23). Matrices for this problem are defined as follows:

$$h_{nm}^{(1)} = \delta_{nm} H_n^{(2)}(kr_0) + \left\{ \sum_{\substack{l=-\infty \\ l \le 0}}^{\infty} H_{n-m}^{(2)}(k2la) - \sum_{l=-\infty}^{\infty} H_{n+m}^{(2)}(l2ka - 2kc) \right\} J_n(kr_0) \tag{36}$$

$$h_{nm}^{(2)} = j^n(-j)^m H_{m-n}^{(2)}(kd) J_n(kr_0) + j^n \left[\sum_{\substack{l=-\infty \\ l \ne 0}}^{\infty} \sum_{p=-\infty}^{\infty} (-j)^p H_{p-m}^{(2)}(l2ka) J_{p-n}(kd) - \sum_{l=-\infty}^{\infty} \sum_{p=-\infty}^{\infty} (-j)^p H_{p+m}^{(2)}(l2ka - 2kc) \cdot J_{p-n}(kd) \right] J_n(kr_0) \tag{37}$$

$$h_{nm}^{(3)} = j^n(-j)^m H_{m-n}^{(2)}(-kd) J_n(kr_1) + j^n \left[\sum_{\substack{l=-\infty \\ l \ne 0}}^{\infty} \sum_{p=-\infty}^{\infty} (-j)^p H_{p-m}^{(2)}(l2ka) \cdot J_{p-n}(-kd) - \sum_{l=-\infty}^{\infty} \sum_{p=-\infty}^{\infty} (-j)^p H_{p+m}^{(2)}(l2ka - 2kc) \cdot J_{p-n}(-kd) \right] J_n(kr_1) \tag{38}$$

$$h_{nm}^{(4)} = \delta_{nm} H_n^{(2)}(kr_1) + \left[\sum_{\substack{l=-\infty \\ l \ne 0}}^{\infty} H_{n-m}^{(2)}(l2ka) - \sum_{l=-\infty}^{\infty} H_{n+m}^{(2)}(l2ka - 2kc) \right] J_n(kr_1) \tag{39}$$

$$c_n^{(a)} = (-1)^{n+1} E_0 \sin\left(\frac{\pi c}{a} - n\alpha\right) J_n(kr_0) \tag{40}$$

$$c_n^{(b)} = (-1)^{n+1} E_0 e^{jk'd} \sin\left(\frac{\pi c}{a} - n\alpha\right) J_n(kr_1) \tag{41}$$

where matrices are of the same dimensions as in Section II-B. Note that subscripts n, m are used here in preference to i, j to avoid confusion with previous equations and with $j = \sqrt{-1}$.

III. Transmission and Reflection Coefficients

Consider an x-directed filament with uniform current I, located at $y = d'$, $z = l$ inside a rectangular waveguide (see Fig. 1). The electric field due to this filament is [4, eq. (21)]

$$E_{x(\text{fil})} = \sum_{m=1}^{\infty} -\frac{jk\eta I}{ak_m} \sin\left(\frac{m\pi d'}{a}\right) \sin\left(\frac{m\pi y}{a}\right) e^{-k_m|z-l|} \tag{42}$$

where

$$k_1 = jk' \quad \text{and} \quad k_m = \sqrt{\left(\frac{m\pi}{a}\right)^2 - k^2}, \quad \text{for } m > 1, \eta = \sqrt{\frac{\mu}{\varepsilon}}.$$

For large z, only the dominant mode is present (assuming that other modes are cutoff) and

$$E_{x(\text{fil})} = -\frac{k\eta I}{k'a} \sin\left(\frac{\pi d'}{a}\right) \sin\left(\frac{\pi y}{a}\right) e^{jk'l} e^{-jk'z} \text{ (large } z\text{)}. \tag{43}$$

Consider the single-post problem of Fig. 1. Post currents are given by (5). Now represent a section of the post with surface current J_x and width $r_0\, d\theta$ as a filament. The elementary contribution to the electric field is

$$dE_x^s = -\frac{k\eta r_0 J_x(\theta)\, d\theta}{k'a} \sin\frac{\pi(c + r_0\cos\theta)}{a} \cdot \sin\left(\frac{\pi y}{a}\right) e^{jk'r_0\sin\theta} e^{-jk'z}, \quad \text{for large } z. \tag{44}$$

Integration over the post yields

$$E_x^s = -\frac{k\eta r_0}{k'a}\sin\left(\frac{\pi y}{a}\right)e^{-jk'z}\int_{-\pi}^{\pi} J_x(\theta) \cdot \sin\frac{\pi(c+r_0\cos\theta)}{a} e^{jk'r_0\sin\theta}\,d\theta \quad (45)$$

where $J_x(\theta)$ is given by (5) and

$$\sin\frac{\pi(c+r_0\cos\theta)}{a} = \sin\left(\frac{\pi c}{a}\right)\cos\left(\frac{\pi r_0\cos\theta}{a}\right)+\cos\left(\frac{\pi c}{a}\right)\sin\left(\frac{\pi r_0\cos\theta}{a}\right).$$

The following results are utilized:

$$I_1 = \int_{-\pi}^{\pi}\cos\left(\frac{\pi r_0\cos\theta}{a}\right) \cdot e^{jk'r_0\sin\theta}e^{jn\theta}\,d\theta = (-1)^n 2\pi J_n(kr_0)\cos(n\alpha)$$

$$I_2 = \int_{-\pi}^{\pi}\sin\left(\frac{\pi r_0\cos\theta}{a}\right) \cdot e^{jk'r\sin\theta}e^{jn\theta}\,d\theta = (-1)^{n+1} 2\pi J_n(kr_0)\sin(n\alpha).$$

The above results are obtained by expressing sine and cosine as exponentials and using the integral form of the Bessel function [17]

$$J_n(x) = \frac{1}{2\pi}\int_{-\pi}^{\pi} e^{j(x\sin\theta - n\theta)}\,d\theta.$$

Equation (7) is applied, and the scattered fields below are obtained

$$E_x^s = \frac{4}{k'a}\sin\left(\frac{\pi y}{a}\right)e^{-jk'z}\sum_{n=-\infty}^{\infty}(-1)^n a_n\sin\left(\frac{\pi c}{a}-n\alpha\right) \quad (46)$$

and the total field E_x for large z is

$$E_x = E_x^i + E_x^s = E_0\sin\left(\frac{\pi y}{a}\right) \cdot e^{-jk'z}\left[1+\frac{4}{E_0k'a}\sum_{n=-\infty}^{\infty}(-1)^n a_n\sin\left(\frac{\pi c}{a}-n\alpha\right)\right]. \quad (47)$$

The transmission coefficient T is

$$T = \frac{E_x}{E_x^i} = 1+\frac{4}{E_0k'a}\sum_{n=-\infty}^{\infty}(-1)^n a_n\sin\left(\frac{\pi c}{a}-n\alpha\right). \quad (48)$$

Similarly, the reflection coefficient Γ can be obtained by changing the sign of the exponent and integrating with respect to θ as above. The result is

$$\Gamma = \frac{4}{E_0k'a}\sum_{n=-\infty}^{\infty} a_n\sin\left(\frac{\pi c}{a}+n\alpha\right). \quad (49)$$

For the triple-post configuration of Fig. 3, the coefficients are

$$T = 1+\frac{4}{E_0k'a}\sum_{n=-\infty}^{\infty}(-1)^n \cdot\left[a_n\cos(n\alpha)+2b_n\sin\left(\frac{\pi c}{a}-n\alpha\right)\right] \quad (50)$$

$$\Gamma = \frac{4}{E_0k'a}\sum_{n=-\infty}^{\infty}\left[a_n\cos(n\alpha)+2b_n\sin\left(\frac{\pi c}{a}+n\alpha\right)\right] \quad (51)$$

and for the single-post array of Fig. 4, coefficients are

$$T = 1+\frac{4}{E_0k'a}\sum_{n=-\infty}^{\infty}(-1)^n\left(a_n+b_ne^{jk'd}\right)\sin\left(\frac{\pi c}{a}-n\alpha\right) \quad (52)$$

$$\Gamma = \frac{4}{E_0k'a}\sum_{n=-\infty}^{\infty}\left(a_n+b_ne^{-jk'd}\right)\sin\left(\frac{\pi c}{a}+n\alpha\right). \quad (53)$$

IV. Reduction of Matrix [H] to Forms Suitable for Computation

Matrix $[H]$ elements, as given in (15), etc., are not suitable for computation because the series involved converges very slowly. The real part of $[H]$ for the single- and triple-post configurations can be expressed in closed form. The imaginary part can be expressed in terms of integrals suitable for rapid numerical evaluation. The results are presented for the single post only. Real ($h_{ij}^{(r)}$) and imaginary ($h_{ij}^{(i)}$) parts of h_{ij} as given in (15) are

$$h_{ij}^{(r)} = \delta_{ij}J_i(kr_0)+\left\{\sum_{\substack{l=-\infty\\ l\neq 0}}^{\infty} J_{i-j}(k2la) - \sum_{l=-\infty}^{\infty} J_{i+j}[k(2la-2c)]\right\}J_i(kr_0) \quad (54)$$

$$h_{ij}^{(i)} = -\delta_{ij}Y_i(kr_0)-\left\{\sum_{\substack{l=-\infty\\ l\neq 0}}^{\infty} Y_{i-j}(k2la) - \sum_{l=-\infty}^{\infty} Y_{i+j}[k(2la-2c)]\right\}J_i(kr_0). \quad (55)$$

Let $h_{ij}^{(r)} = \hat{h}_{ij}^{(r)}\cdot J_i(kr_0)$, $h_{ij}^{(i)} = \hat{h}_{ij}^{(i)}J_i(kr_0)$. Then

$$\hat{h}_{ij}^{(r)} = \hat{h}_{ji}^{(r)}, \qquad \hat{h}_{ij}^{(i)} = \hat{h}_{ji}^{(i)}.$$

The real part may be evaluated in general, as follows, if only the dominant mode propagates ($\pi < ka < 2\pi$):

$$\hat{h}_{ij}^{(r)} = \hat{h}_{ji}^{(r)} = \begin{cases} -D\cos\left[\dfrac{(i+j)\pi}{2}+\dfrac{2c\pi}{a}\right]\cos\left[(i+j)\left(\dfrac{\pi}{2}-\alpha\right)\right], & \text{for } |i-j| \text{ odd} \\ D\{\cos\}(i-j)\alpha-\cos\left[\dfrac{(i+j)\pi}{2}+\dfrac{2c\pi}{a}\right]\cos\left[(i+j)\left(\dfrac{\pi}{2}-\alpha\right)\right], & \text{for } |i-j| \text{ even} \end{cases} \quad (56)$$

where

$$D = \frac{2}{\sqrt{(ka)^2-\pi^2}} = \frac{2}{k'a}$$

$$\alpha = \sin^{-1}\left(\frac{\pi}{ka}\right) = \tan^{-1}\left(\frac{\pi}{k'a}\right).$$

If the post is at the center of the waveguide ($c = a/2$), (56) becomes

$$\hat{h}_{ij}^{(r)} = \hat{h}_{ji}^{(r)} = \begin{cases} 0, & \text{for } |i-j| \text{ odd} \\ 2D\cos(i\alpha)\cos(j\alpha), & \text{for } |i-j| \text{ even} \end{cases}. \tag{57}$$

Equation (56) above is obtained by using an integral form of the Bessel function and various manipulations. Details are given in [20]. The imaginary part may be evaluated as follows:

$$\hat{h}_{ij}^{(i)} = \begin{cases} \dfrac{2}{\pi}\left[\displaystyle\int_0^{\pi/2} f_1(t)\,dt + \int_0^{\infty} f_2(t)\,dt\right], & \text{for } |i-j| \text{ odd} \\ -\delta_{ij}\dfrac{Y_i(kr_0)}{J_i(kr_0)} + \dfrac{2}{\pi}\left[\displaystyle\int_0^{\pi/2} f_3(t)\,dt + \int_0^{\infty} f_4(t)\,dt\right], & \text{for } |i-j| \text{ even} \end{cases} \tag{58}$$

where

$$f_1(t) = \frac{\sin[(ka-2kc)\sin t]\sin(i+j)t}{\sin(ka\sin t)} \tag{59a}$$

$$f_2(t) = \frac{\sinh[(ka-2kc)\sinh t]\sinh(i+j)t}{\sinh(ka\sin ht)} \tag{59b}$$

$$f_3(t) = \frac{\cos[(ka-2kc)\sin t]\cos(i+j)t - \cos(ka\sin t)\cos(i-j)t}{\sin(ka\sin t)} \tag{59c}$$

$$f_4(t) = \frac{\cosh(i-j)te^{-ka\sinh t} - \cosh(i+j)t\cosh[(ka-2kc)\sin ht]}{\sinh(ka\sinh t)}. \tag{59d}$$

Equation (58) is obtained by using an integral form of the Neumann function and various manipulations. Details are given in [20]. Series forms for (54) and (55) are given by Williamson [11].

The integrals $\int_0^{\pi/2} f_p(t)\,dt$, ($p = 1, 3$) are improper since there are poles in the interval $(0, \pi/2)$. However, the Cauchy principal value may be obtained by subtracting from and adding to the original functions $f_p(t)$ a selected term, thereby changing the poles to removable singularities. Two other integrals are improper because of an infinite range of integration. However, the integrand in each case decreases rapidly with increasing t; the integrals may be evaluated over a finite interval and the error involved may be specified.

The reduction of matrix $[H]$ for the triple-post configuration is quite similar to that outlined above. For the single-post array of Fig. 4, the reduction is more complex but proceeds along somewhat similar lines. In this case, integrals are required for both real and imaginary parts. Details are given in [20].

V. Results

Computer programs have been prepared to carry out the analysis of the preceding sections. Listings are included in [20]. Errors in the various portions of the programs and N, which determines the number of terms of the Fourier series, may be specified. Program listings may be obtained from the authors.

Data for the centered and off-center single-post obstacle have been computed. These agree precisely (within better than 1 percent) with the data in Marcuvitz and that of [16] for larger posts. Figs. 5 and 6 show normalized reactances $(x_a/z_0)(\lambda_g/2a)$ and $(x_b/z_0)(\lambda_g/2a)$ of the triple-post configuration. The configurations of Fig. 5, with post axes equally separated from each other and from waveguide walls, is one which is commonly used in triple-post filter design. The geometry of Fig. 6 corresponds to equal spacing of all images. Data are given for various frequencies and post sizes, curves for $\lambda/a = 1.01$ and 1.99 describe behavior just above TE_{10} and just below TE_{20} mode cutoff, respectively. Note that data are independent of waveguide ratio b/a. The data for the single-post obstacle indicated dispersion of the curve for $(x_b/z_0)(\lambda_g/2a)$ and for $d/a > 0.25$. Note that dispersion occurs for smaller posts in Figs. 5 and 6, as expected. Furthermore, dispersion occurs approximately for $d/a > 0.11$ in Fig. 5 and for $d/a > 0.15$ in Fig. 6. The minimum image spacing is larger for Fig. 6 than for Fig. 5. It is noted also that the triple-post dispersion for $(x_a/z_0)(\lambda_g/2a)$ is considerably smaller than that of the single post. The data of Figs. 5 and 6 also has been compared with that of the multifilament method [16]. Agreement is better than 1 percent. Fig. 7 shows computed transmission coefficient data for a two-element post filter. The solid curve shows the complete data with all interactions taken into account. The dotted curve (approximate solution) shows the result of computation which neglects the higher order (cutoff) mode interactions between posts. In other words, the dotted curve corresponds to results obtained by cascading single-post equivalent circuits, such as those presented in [16]. The higher order mode interactions become more significant as post size increases. Fig. 7 shows an appreciable difference between curves, even though the spacing is larger than a half-wavelength. Higher order mode interactions therefore may be neglected, except in cases of extremely high Q; even in those cases, the fractional shift of center frequency may be very small (see

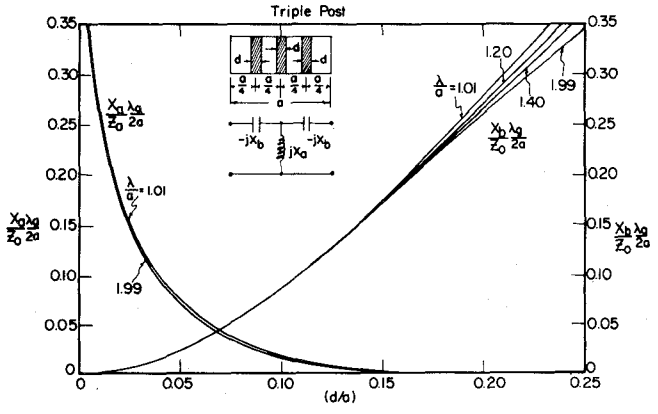

Fig. 5. Equivalent circuit for the triple-post obstacle (uniform spacing, identical posts).

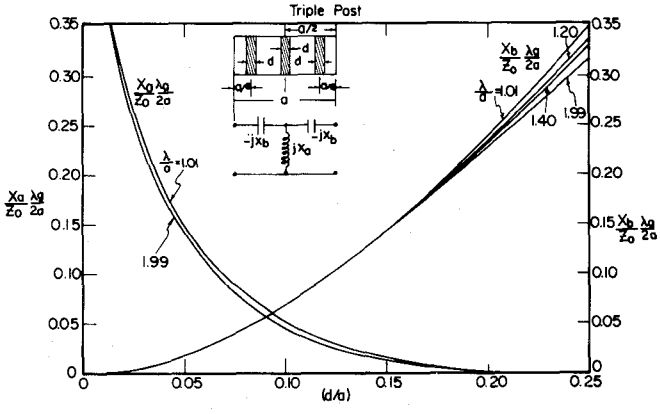

Fig. 6. Equivalent circuit for the triple-post obstacle (uniform image spacing, identical posts).

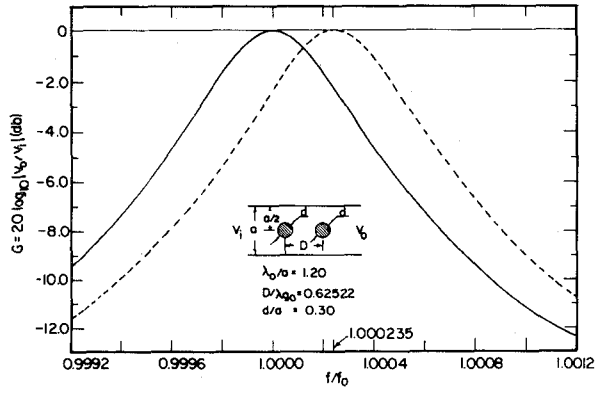

Fig. 7. Filter response (transmission coefficient) of a single-post array ($d/a = 0.30$).

Fig. 7). Similar results (not shown) have been obtained for triple-post arrays. These show less effect of higher order mode interactions in accordance with [3].

VI. Conclusion

A complete analysis of cylindrical post structures in rectangular waveguides has been developed. As many Fourier series terms ($e^{jn\theta}$) as desired may be taken into account. All higher order mode interactions between posts are considered. Computations are rapid and accurate. Errors are controlled as part of the computer program. Data is presented for triple-post configurations and for a two-post filter.

References

[1] D. S. Saxon, *Notes on lectures by Julian Schwinger: Discontinuities in waveguides*, University Microfilms, Ann Arbor, MI.

[2] N. Marcuvitz, *Waveguide Handbook*, M.I.T. Rad. Lab. Series, vol. 10. New York: McGraw-Hill, 1951, pp. 257–262.

[3] G. Craven and L. Lewin, "Design of microwave filters with quarter-wave couplings," *J. IEE*, vol. 103(b), pp. 173–177, 1956.

[4] L. Lewin, *Theory of Waveguides*. New York: Wiley, 1975.

[5] E. A. Mariani, "Designing narrow-band triple-post waveguide filters," *Microwaves*, vol. 4, 1965, pp. 93–97. See also "Design of narrow-band, direct-coupled waveguide filters using triple-post inductive obstacles," Tech. Rep. ECOM-2566, U.S. Army Electronics Command, Fort Monmouth, NJ, Mar. 1965.

[6] T. A. Abele, "Inductive post arrays in rectangular waveguide," *Bell Syst. Tech. J.*, vol. 57, pp. 577–594, Mar. 1978.

[7] A. V. Moschinskiy and V. K. Berezovskiy, "An exact solution of the problem of scattering of the H_{10} mode on a circular cylindrical inhomogeneity in a rectangular waveguide," *Radio Eng. Electron. Phys.*, vol. 22, pp. 18–22, July 1977.

[8] J. E. Joshi and J. A. F. Cornick, "Analysis of waveguide post configurations: Part II—Dual-gap cases," *IEEE Trans. Microwave Theory Tech.*, vol. MTT-25, pp. 173–181, Mar. 1977.

[9] R. L. Eisenhart and P. J. Khan, "Theoretical and experimental analysis of a waveguide mounting structure," *IEEE Trans. Microwave Theory Tech.*, vol. MTT-19, pp. 706–719, Aug. 1971.

[10] R. G. Hicks and P. J. Khan, "Improved waveguide diode mount circuit model using post equivalence factor analysis," *IEEE Trans. Microwave Theory Tech.*, vol. MTT-30, pp. 1914–1920, Nov. 1982.

[11] A. G. Williamson and D. V. Otto, "Analysis of a waveguide mounting structure," in *Proc. I.R.E.E. Australian Electronics Communications*, Apr. 1973, pp. 95–97. See also A. G. Williamson, "Contributions to the theory of cylindrical antennas in a rectangular waveguide." Ph.D. thesis, Univ. of Auckland, New Zealand, 1976.

[12] N. Okamoto, I. Nishioka, and Y. Nakanishi, "Scattering by a ferrimagnetic circular cylinder in a rectangular waveguide," *IEEE Trans. Microwave Theory Tech.*, vol. MTT-19, pp. 521–527, June 1971.

[13] L. Lewin, "Solution of a singular integral equation over a multiple interval and applications to multiple strips, grids and waveguide diaphrams," *Electron. Lett.*, vol. 2, pp. 458–459, 1966.

[14] K. Chang and P. J. Kahn, "Analysis of three narrow transverse strips in waveguide," in *1978 IEEE-MTT-S Microwave Symp. Dig. Tech. Pap.*, pp. 419–421.

[15] R. H. Harrington, *Field Computation by Moment Methods*. New York: Macmillan, 1968.

[16] Y. Leviatan, P. Li, A. T. Adams, and J. Perini, "Single-post inductive obstacles in rectangular waveguides," *IEEE Trans. Microwave Theory Tech.*, vol. MTT-31, pp. 806–811, Oct. 1983.

[17] R. V. Churchill and J. W. Brown, *Fourier Series and Boundary Value Problems*, 3rd Ed. New York: McGraw-Hill, 1978, pp. 186–190.

[18] R. F. Harrington, *Time-Harmonic Electromagnetic Fields*. New York: McGraw-Hill, 1961, pp. 50, 66, 227.

[19] Jahnke-Emde-Lösch, *Tables of Higher Functions*, 6th Ed. New York: McGraw-Hill, 1960, pp. 146-147, 155.

[20] P. Li, A. T. Adams, Y. Leviatan, and J. Perini, "Multiple-post inductive obstacles in rectangular waveguide," Report TR-83-11, Dept. Electrical and Computer Eng., Syracuse Univ., June, 1983.

[21] R. E. Collin, *Field Theory of Guided Waves*. New York: McGraw-Hill, 1960, p. 200.

✤

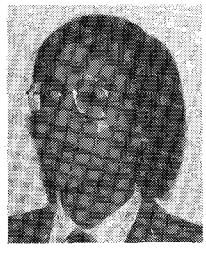

Ping Guan Li was born in 1945 in Changle County, Fukien Province, China. He graduated from the Department of Radio-Electronics, Tsinghua University, People's Republic of China, in February, 1968. He came to the United States in 1981 for postgraduate studies at Syracuse University where he received the M.S. degree in 1982. He is now working toward the Ph.D. degree under the guidance of Professor A. T. Adams of Syracuse University.

Arlon T. Adams (M'58–SM'72) received the B.A. degree in applied science from Harvard University, Cambridge, MA in 1953, and the M.S. and Ph.D. degrees in electrical engineering in 1961 and 1964, respectively, both from the University of Michigan, Ann Arbor.

He served as a Line Officer in the Atlantic Destroyer Fleet from 1953 to 1957, and until 1959, he was employed by Sperry Gyroscope Company, Long Island, NY. From 1959 to 1963, he was a Graduate Research Associate at the University of Michigan, Ann Arbor. In 1963, he joined the Faculty of Syracuse University, Syracuse, NY, where he is presently Professor of Electrical Engineering. During the academic year 1976–1977, he was a Visiting Scholar at the University of California at Berkeley where he worked on infrared antennas. His current interests are in numerical methods for electromagnetic problems. He is the author of a textbook on electromagnetic theory, coauthor of a textbook on electromagnetic compatibility, and has published over 70 papers on electromagnetics.

✤

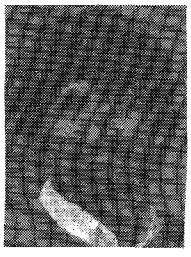

Yehuda Leviatan (S'81–M'82) was born in Jerusalem, Israel, on September 19, 1951. He received the B.Sc. and M.Sc. degrees in electrical engineering from the Technion-Israel Institute of Technology, Haifa, Israel, in 1977 and 1979, respectively, and the Ph.D. degree in electrical engineering from Syracuse University, Syracuse, NY, in 1982.

He held a Teaching Assistantship during his graduate work from 1977 to 1979 at the Technion, a Research Assistantship during his graduate work from 1979 to 1981 at Syracuse University, and a Postdoctoral Research position at Syracuse University during the summer of 1982. From 1980–1982, he was also engaged as a part-time Research Engineer at the Syracuse Research Corporation. In September 1982, he joined the Faculty of the Electrical and Computer Engineering Department at Syracuse University as an Assistant Professor. He provides consulting services to the Syracuse Research Corporation and to IBM. His research interests are in the areas of mathematical and numerical methods applied to antennas, transmission lines, and waveguides, scattering and transmission through apertures, near fields of radiating systems, and adaptive arrays.

✤

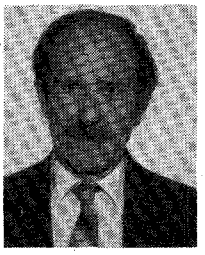

Jose Perini (M'61–SM'76) was born in São Paulo, Brazil. He received the B.S. degree in electrical and mechanical engineering from Escola Politecnica de São Paulo, São Paulo, Brazil, in 1952.

Subsequently, he worked for Real Transportes Aeroes, a Brazilian airline company, for three years, as Manager for Radio Maintenance, and in the last six months, as Assistant to the Manager of General Maintenance. In 1955, he joined the Electrical Engineering Department of Escola Politecnica de São Paulo, as an Assistant Professor, teaching until 1958. During this time, he also conducted ionospheric research. He received the Ph.D. degree in electrical engineering from Syracuse University, Syracuse, NY, in 1961. From 1959 to 1961, while studying at Syracuse, he was also a consultant for General Electric (G.E.) Co. in the Television Transmitting Antenna area. His Ph.D. dissertation was derived from this work. In 1961, he returned to Brazil as an Associate Professor of Electrical Engineering at Escola Politecnica de São Paulo and also as a consultant for G.E. of Brazil. In September 1962, he became Assistant Professor of Electrical Engineering at Syracuse University, where he was promoted to Associate Professor in 1966 and to Professor in 1971. He rejoined G.E. in Syracuse as a consultant in the same area of TV transmitting antennas until 1969. He has had many research contracts with the Navy, Air Force, and Army. He has consulted extensively in the U.S. and abroad in the areas of electromagnetics and communications. He has many published papers in the fields of antennas, microwaves, EMC, and circuit theory. He also holds two patents on TV transmitting antennas.

Theory and Numerical Modeling of a Compact Low-Field High-Frequency Gyrotron

PETER VITELLO, WILLIAM H. MINER, AND ADAM T. DROBOT

Abstract—**The electron-cyclotron maser interaction provides an extremely efficient means of generating high-power radiation in the millimeter and submillimeter regimes. For devices where both high frequencies and low magnetic fields are required, high cyclotron-harmonic interactions must be considered. We present here a linear and nonlinear analysis of a TE_{m11} whispering-gallery-mode gyrotron. Resonances at the mth and $(m \pm 1)$th cyclotron harmonic are found. The start oscillation condition is calculated from linear theory for a wide range of parameters. Maximum efficiency for different beam and cavity conditions is calculated with a fully relativistic numerical simulation code. High efficiencies, > 35 percent, have been found at the mth cyclotron harmonic. The effect on the efficiency of an initial velocity spread in the electron beam has also been considered.**

Manuscript received June 6, 1983; revised November 28, 1983. This work was supported in part by UCLA under Contract 400001 and in part by the U.S. Army Research Office, Triangle Research Park, NC, under Contract DAAG29-82-K-0004.

P. Vitello and A. Drobot are with Science Applications, Inc., McLean, VA 22102.

W. Miner is with the Fusion Research Center, University of Texas at Austin, Austin, TX 78712.

I. Introduction

THE ELECTRON-CYCLOTRON maser interaction provides perhaps one of the most efficient mechanisms for generating continuous high-power radiation in the millimeter and submillimeter regimes [1]–[6]. The interaction takes place between the electromagnetic (RF) waves of a cavity or waveguide, and an electron beam in which the electrons comprising the beam move along individual

0018-9480/84/0400-0373$01.00 ©1984 IEEE